Biol. Cybern. 83, L1–L9 (2000)

Biological Cybernetics

Letter to the editors

Lateral spike conduction velocity in the visual cortex affects spatial range of synchronization and receptive field size without visual experience: a learning model with spiking neurons

Mirko Saam, Reinhard Eckhorn

Neurophysics Group, Physics Department, Philipps University, 35032 Marburg, Germany

Received: 19 November 1999 / Accepted in revised form: 14 April 2000

Abstract. Classical receptive fields (cRF) increase in size from the retina to higher visual centers. The present work shows how temporal properties, in particular lateral spike velocity and spike input correlation, can affect cRF size and position without visual experience. We demonstrate how these properties are related to the spatial range of cortical synchronization if Hebbian learning dominates early development. For this, a largely reduced model of two successive levels of the visual cortex is developed (e.g., areas V1 and V2). It consists of retinotopic networks of spiking neurons with constant spike velocity in lateral connections. Feedforward connections between level 1 and 2 are additive and determine cRF size and shape, while lateral connections within level 1 are modulatory and affect the cortical range of synchronization. Input during development is mimicked by spike trains with spatially homogeneous properties and a confined temporal correlation width. During learning, the homogeneous lateral coupling shrinks to limited coupling structures defining synchronization and related association fields (AF). The size of level-1 synchronization fields determines the lateral coupling range of developing level-1-to-2 connections and, thus, the size of level-2 cRFs, even if the feedforward connections have distance-independent delays. AFs and cRFs increase with spike velocity in the lateral network and temporal correlation width of the input. Our results suggest that AF size of V1 and cRF size of V2 neurons are confined during learning by the temporal width of input correlations and the spike velocity in lateral connections without the need of visual experience. During learning from visual experience, a similar influence of AF size on the cRF size may be operative at successive levels of processing, including other parts of the visual system.

Correspondence to: R. Eckhorn
(e-mail: Reinhard.Eckhorn@physik.uni-marburg.de)

1 Introduction

1.1 Receptive and association fields

The best explored and most accepted concept of visual processing is that of the classical receptive field (cRF; Hubel and Wiesel 1962) which characterizes the spatio-temporal coupling between small visual stimuli and the spike response of single visual neurons. Less intensely investigated is the influence of visual context outside the cRF. Context can modulate the cRF properties strongly over a broad range in visual space (Allman et al. 1985). In recent years synchronization fields were found in the lower areas of the visual cortex. Their size has been defined by the cortical extent of coherence among fast cortical oscillations (35–90 Hz; Eckhorn 1994; Frien and Eckhorn 2000). According to the cRFs of single neurons, the projections of synchronization fields to visual space have been termed the association fields (AF; Eckhorn et al. 1990) or context fields (Phillips and Singer 1997) of local groups of neurons. One intensely discussed hypothesis for the AFs' function is that feature grouping is supported in their field by synchronizing those neurons currently representing the same visual object (reviews in Eckhorn 1999; Gray 1999).

Grouping of features into whole objects may also be coded by the convergence of their relevant feature detectors (Barlow 1972; Riesenhuber and Poggio 1999). If convergence is present over all levels of visual processing, it would produce a systematic increase in cRF size from retina to higher centers. This principle may become operative during early visual experience if objects to be learned appear transiently and alone in a scene. The component feature detectors of an object would be co-activated, and Hebbian learning could establish stable convergent connections. However, real visual objects are parts of complex scenes and their segregation from other objects is a formidable problem. One potential solution for scene segmentation is provided by the concept of transient synchronization within the representational range of an object. In such a scheme, Hebbian learning would only stabilize feedforward connections of

synchronized inputs. In this way, the synchronization and related association field at a lower level would determine the cRF type and size at the next level of processing and hence, cRFs would increase within the hierarchy of visual cortical areas.

1.2 Input to visual cortex during development

Evidence of cortical plasticity by visual experience is rarely disputed (e.g., Hubel and Wiesel 1970; Crair et al. 1998). However, many functional units of the visual cortex emerge before eye opening, demonstrating that visual experience is not required for initial development (Crair et al. 1998; Chapman et al. 1999). Spike activities, already present in the retina before eye opening, probably provide instructive cues for guiding the development within the striate cortex (Weliky and Katz 1999). This activity consists of stochastic spike trains, simultaneously modulated in their rates over large retinal regions (Meister et al. 1991; Wong and Oakley 1996). For the present model we assume (as a working hypothesis) precise correlations (2–10 ms) among inputs to the V1 level over ranges of several hypercolumns. This seems reasonable because activities in the developing retina are dominated by tight junctions among neighboring neurons (Penn et al. 1994), which are known to mediate fast electrical coupling in the millisecond scale. Precise temporal structuring of cortical input may also be introduced by rhythmic cortico–thalamic feedback (5–10 Hz) and via fast intracortical inhibition (20–30 Hz). Thus, precise correlations in maintained activities at thalamic and primary cortical levels are probably present before visual experience and may guide the early development of connectivity patterns.

1.3 Hebbian learning supports the emergence of functional cortical units during development

Several correlational properties of afferent spike trains to the striate cortex are consistent with predictions of activity-dependent models of cortical map and cRF development in V1 before eye opening. One model proposes that the observed differences in correlated firing between ON- and OFF-thalamic afferents can drive the segregation of a simple cell's cRF subregions (Miller 1994). Other models show that the competing requirements of joint ocular dominance and orientation map development in V1 can be resolved if within-eye activity is more strongly correlated than between-eye activity (Miyashita et al. 1997; Stetter et al. 1997), a fact that has recently been confirmed experimentally (Weliky and Katz 1999).

Most models of striate cortical development based on Hebbian learning use partially synchronized input activities, while few assume differences in delays. For instance, Gerstner et al. (1996) explain the temporal precision in auditory direction discrimination by sorting out axons of differing delays by correlation learning, resulting in coincident spikes. Other recent work assumes correlation-dependent learning of synaptic delays by a rule decreasing the correlation delays in synaptic signals and generating coincident inputs (Hüning et al. 1998; Eurich et al. 1999). Finally, Ritz et al. (1994) demonstrate that the average activation delay among reciprocally connected excitatory neurons restricts the size of cortical synchronization fields in which zero-delay phase-locking is possible for a given oscillation frequency.

In our present model of visual areas V1 and V2, the main properties are lateral spike conduction delays increasing systematically with distance, in addition to partial correlations of the external signals. Their relevance is tested for the emergence of functional cortical units without visual experience (an abstract was published in Saam et al. 1999).

2 Methods

2.1 Model neuron

We use pulse coding model neurons with spike inputs, realistic post synaptic potentials, and an adaptive spike encoder with dynamic threshold (Eckhorn et al. 1990). The input part of a neuron n_i consists of synapses S_{ij}, which have an impulse response $h(t)$ and a synaptic efficacy w_{ij}.

$$S_{ij}(t) = w_{ij}^{S} I_j(t - \Delta_{ij}) * h(t, \tau_{S1}, \tau_{S2}) \ , \tag{1}$$

where $*$ denotes the convolution operator, i is the index of the postsynaptic neuron n_i, I_j the spike output of a presynaptic neuron n_j, and Δ_{ij} the conduction delay for spikes between n_i and n_j. The synaptic response $h(t)$ is modeled by a second-order leaky integrator:

$$h(t, \tau_1, \tau_2) = \mathrm{H}(t)(\exp(-t/\tau_2) - \exp(-t/\tau_1)) \ . \tag{2}$$

$\mathrm{H}(\cdot)$ denotes the Heaviside function. Time constants are chosen such that the excitatory postsynaptic potential (EPSP) reaches its maximum value at $t = 1$. Two types of inputs are processed separately: external feeding input F_{ij} and lateral linking input L_{ij} (Eckhorn et al. 1990).

$$S_i(t) = \sum_j S_{ij}(t) \ , \tag{3}$$

where S may be F or L. While the feeding inputs F_i have conventional synapses (non-NMDA), the linking inputs L_i exert multiplicative influence on the feeding inputs. The resulting membrane potential, driving the spike encoder, is therefore calculated as:

$$U_i(t) = F_i(t) \cdot (1 + L_i(t)) \ , \tag{4}$$

which enables the feeding input to drive the spike encoder even with zero linking input, while the reverse is not possible. Multiplicative interactions have been chosen for the following reasons: Lateral interactions in developing visual cortex area V1 are mainly located in the upper layers where synapses are dominated by NMDA channels (Fox et al. 1989). In V1, NMDA

channels have been reported to mediate gain control, due to their voltage dependences and the differences in the Hill coefficients for binding glutamate at the NMDA receptors. Both properties affect the response to afferent visual input in a graded multiplicative fashion (Fox and Daw 1992). Thus, a multiplicative interaction among forward and lateral connections seems biologically plausible. In our model, this modulatory action of the linking on the feeding inputs ensures that the local coding of single neurons (here the cRF) is not deteriorated by lateral connections (Eckhorn et al. 1990).

In the spike encoder, the membrane potential $U_i(t)$ is compared to a threshold $\theta_i(t)$. If $U_i(t)$ exceeds $\theta_i(t)$, a spike is generated:

$$O_i(t) = \mathrm{H}(U_i(t) - \theta_i(t)) \ . \tag{5}$$

The threshold $\theta_i(t)$ has a static offset value θ_0 and a dynamic part, which is an impulse response of two leaky integrators to the spike output $O_i(t)$:

$$\theta_i(t) = \theta_0 + O_i(t) * [(V_{\theta r}\exp(-t/\tau_{\theta r}) + V_{\theta s}\exp(-t/\tau_{\theta s}))\mathrm{H}(t)] \ . \tag{6}$$

One leaky integrator has an amplitude $V_{\theta r}$ and a short time constant $\tau_{\theta r}$ modeling fast refractory components, while the other ($V_{\theta s}$, $\tau_{\theta s}$) is slower, mimicking spike rate adaptation. Additionally, an absolute refractory period of 1 ms is introduced. The above equations are solved for different temporal resolutions ($\Delta t = 0.2, 0.5, 1.0$). The higher resolutions are important for realizing precise distance-dependent delays in the network. A physiologically realistic time scale is 1 ms for $\Delta t = 1$.

2.2 Network topology and signal properties

Level 1 and 2 each consist of 441 neurons arranged on a two-dimensional Cartesian grid. To avoid artifacts from boundaries, toroidal boundary conditions are used. All neurons have the same time constants and threshold properties (Table 1). We expected complex intermingled effects on the learning process in lateral and feedforward synapses by the different types of temporal spike dispersion, including the partial correlation of the stochastic external inputs and the systematic delay dispersion in lateral and feedforward axons. In order to keep these effects separate we built and analyzed the model in three consecutive steps (Fig. 1: scenario A, B, and C).

2.2.1 Scenario A: Learning the level-1 linking synapses of lateral connections with distance-dependent delays (Fig. 1). Lateral axons project to neighbors up to a distance of 10 neurons. The initial strengths w_c of these linking synapses are low and chosen randomly. The axons transmit spikes at constant velocity v_{ax} (Table 1) so that delays increase proportional to lateral distance (for the choice of realistic velocities see the Discussion). Other delays, including synaptic and dendritic ones, are assumed to be constant in their average values so that their sum Δ_0 is also constant and can be compensated in the present simulations by a temporal offset Δ_0 in the learning function (arguments for these simplifications are given in the Discussion).

Table 1. Network parameters

Neuron parameters			
τ_{f1}	0.2789 ms	τ_{f2}	9.0 ms
τ_{l1}	0.3866 ms	τ_{l2}	4.0 ms
θ_0	0.3	v_{ax}	1.0 grid/ms
$V_{\theta r}$	5.0	$\tau_{\theta r}$	5.0 ms
$V_{\theta s}$	1.0	$\tau_{\theta s}$	80.0 ms
m_{GWN}	1.0	σ_{GWN}	0.3
Learning level-1 connections (scenario A)			
p_p	0.25	f_p	10.0 Hz
σ_p	2.5 ms	w_c	0.005
τ_{p1}	0.3866 ms	τ_{p2}	4.0 ms
α	0.15	γ	0.005
Learning level-1-to-level-2 connections (scenarios B, C)			
A_{12}	0.03	σ_{12}	6.0 grid units
f_b	10.0 Hz	v_b	1.0 grid/ms
τ_{p1}	0.2789 ms	τ_{p2}	9.0 ms
α	0.25	γ	0.005

The external input to level-1 neurons has no spatial structure in its correlation properties because here we are interested in the effects of lateral transmission delays on the formation of spatially confined coupling structures during learning. Therefore, we composed the input of the following components: (1) Independent Gaussian white noise (GWN) is directly superimposed on the feeding potential with the same mean m_{GWN} and standard deviation σ_{GWN} for all neurons. These continuous signals resemble the postsynaptic potentials evoked by a large number of statistically independent spike trains (Fig. 2a). (2) Correlated spike trains with a Poissonian interval distribution (mean rate f_p) are applied to a fraction (p_p) of all neurons (randomly selected for each correlated burst of activation). These spike trains are temporally correlated (Fig. 2b) according to a common modulation by a Gaussian impulse probability (SD: σ_p). Thus, the input has weak paired spike correlations with a peak at zero time shift and a correlation width of $2\sigma_p$. Despite the presence of the independent GWN, the input spike trains reproduce their mutual correlations approximately among the neurons' outputs (Fig. 2c,d). These are the spike trains

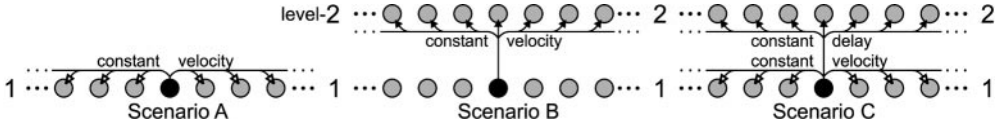

Fig. 1. One-dimensional sketch of the connectivity scheme for a single level-1 neuron in the three different scenarios A, B, and C. *Open arrow heads*: linking synapses; *filled*: feeding synapses

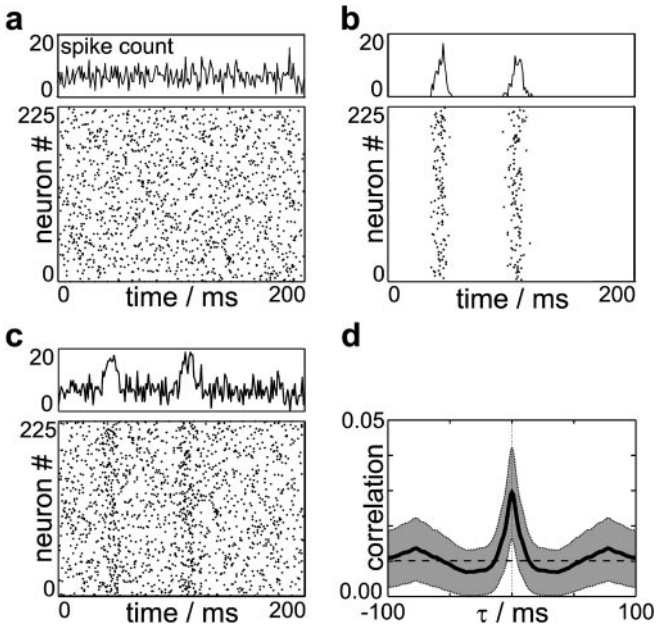

Fig. 2a–d. Scenario A, B: Statistical properties of the spike trains at the output of level 1 that are effective during learning. **a** *Lower panel*: spike patterns of level-1 neurons (each *dot* denotes the occurrence of a spike) and temporal spike count of all neurons (*upper panel*), driven exclusively by the independent Gaussian white noise (GWN) at the inputs. **b** Correlated spike patterns and temporal spike count at the output of level-1 neurons; two events of modulation in spike rate are shown. **c** Spike patterns and temporal spike count at the output of level-1 neurons if GWN (**a**) and the spike patterns (**b**) drive their inputs. Such spike patterns are effective during learning of the lateral linking connections at level 1 and the level-1-to-2 feeding connections. Note that the statistical properties of these signals are spatially homogeneous. **d** Cross-coincidence histogram among pairs of output spike trains, averaged over all combinations of level-1 neurons

that affect learning in the linking synapses after being delayed in the lateral axons.

2.2.2 Scenario B: Learning of level-1-to-2 feeding projections with distance-dependent delays while lateral connections at level 1 are absent (Fig. 1). Here, the effect of delays in feedforward connections is studied in isolation (without the influence of level-1 delays). Level-1 neurons project completely onto level-2 neurons. The initial strengths of the feeding synapses are randomly distributed around a common mean (Fig. 7a) sufficient for initiating spikes in level-2 neurons. Level-1-to-2 axons have the same increase in delays with lateral distance as in scenario A (i.e., constant axonal velocity). The interareal delay between all retinotopically corresponding positions is assumed to be equal. A constant delay does not change the relative timing of incoming spikes at level-2 neurons, and since there is no feedback in our simplified model, this additional delay will have no influence on the learning results. Hence, the effective input spike trains for learning the level-2 synapses have the same statistical properties as those for learning the lateral linking connections at level 1 in scenario A (because they are collaterals of the same layer-1 neurons). This means, that their correlations (Fig. 2d) are spatially homogeneous.

2.2.3 Scenario C: Learning level-1-to-2 feeding connections with constant axonal delay and input from the learned version of level 1 (Fig. 1). Here we test the temporal effects emerging in a learned version of level 1 (scenario A) on feedforward convergent projections to the next level. To obtain separable effects, we kept all delays from level 1 to 2 identical. Level-1 neurons project retinotopically to level-2 neurons, initially with a broad Gaussian weight function (A_{12}, SD: σ_{12}), modeling the large diverging axonal trees present during development. To exclude the possibility that learning results arise from initialization, we trained the network with independent noise inputs as a control. In these simulations all weights decreased below 10^{-5}, which is three decades below the effects obtained with temporally correlated input.

If the learned version of level 1 (scenario A) is excited by a localized activity blob at random positions, damped traveling waves of laterally propagated activity are evoked, conducted by the constant velocity connections. To obtain a more precise control over this wave-like input to level 2 we replaced the lateral level-1 connectivity and its input spike trains by a simulated version of the level-1 outputs with a well defined firing probability:

$$p(r,t) = \exp(-r^2/(2\sigma_b^2))\delta(v_b t - r) \ . \tag{7}$$

Here, r denotes the distance of the neuron from the center of the input blob, v_b is the velocity of a wave front and t the time relative to the occurrence of the blob. During learning, the centers of these wave-like activations are uniformly distributed over the neural grid, chosen in a random sequence with Poissonian interval distribution at a rate f_b.

2.3 Learning

We use a temporal Hebbian learning rule similar to that of a recent work (Gerstner et al. 1996). The weight changes exclusively depend on the relative timing of pre- and postsynaptic spikes in the following way. Each presynaptic spike initiates a synaptic learning potential

$$L_{ij}(t) = O_j(t - \Delta_{ij}) * h(-t, \tau_{p1}, \tau_{p2}) - \alpha \ . \tag{8}$$

The time course of L_{ij} in response to a single presynaptic spike is shown in Fig. 3. If the postsynaptic neuron generates a spike, the synaptic efficacies are changed according to the present values of the learning potentials:

$$\Delta w_{ij}(t) = \max\{\gamma L_{ij}(t) O_i(t), -w_{ij}(t)\} \ , \tag{9}$$

$$w_{ij}(t + \Delta t) = w_{ij}(t) + \Delta w_{ij}(t) \ , \tag{10}$$

where γ denotes the learning rate. With this rule, weights cannot change their sign and it ensures that causality plays a prominent role. With the parameters given in Table 1 the effective duration of the facilitatory (positive) part of the learning window is about 10 ms. The overall learning process lasted 100 000 ms.

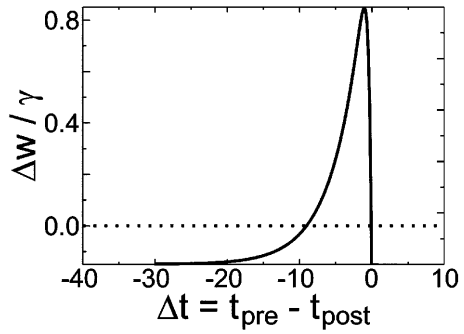

Fig. 3. Synaptic weight change $\Delta w/\gamma$ as a function of the relative timing Δt (in milliseconds) between presynaptic t_{pre} and postsynaptic firing t_{post}

To measure the signal correlations introduced by the learned lateral connections of level 1, their neurons are activated by the same input as during learning. Cycling artifacts are avoided by open boundary conditions and the restriction in calculating the cross-coincidence histograms (CCH) to the spike trains of the central neurons. The spatial strength profile of signal coupling is quantified by a single correlation index from CCHs among neurons of different distances (Juergens and Eckhorn 1997). This index measures the coupling-related area of the central peak and yields values from 0 (uncorrelated) to 1 (completely correlated).

3 Results

3.1 Learning of lateral linking connections (scenario A)

3.1.1 Emergence of lateral coupling kernels. Learning of the lateral linking connections is achieved with temporally correlated input, lacking any spatial structure (Fig. 2c, and see Sect. 2.2). The cross-coincidence histogram among outputs of level-1 neurons (Fig. 2d) shows an average coupling width similar to that of the inputs (not shown). With these outputs affecting learning of the lateral connections, several new spatial network properties emerge. Most important is the laterally restricted coupling kernel with strong weights to direct neighbors and a monotonous decline with increasing distance (Fig. 4a). The confined coupling structures cause a related spatial restriction in the correlations of the spike trains (Fig. 4b). More precisely, the half height width of the spatial distribution of the correlation index varies proportionally with the width D of the lateral coupling kernel.

This confined coupling emerges due to combined interactions of the distance-dependent spike delays and the temporal jitter of the input correlations in conjunction with the learning window. To understand this, consider the probabilities of relative spike timings at the learned synapses. Assume for the noiseless case that each neuron has a temporal Gaussian probability distribution $u(\Delta t)$ to fire with other neurons during the events of simultaneous input modulations according to Fig. 2b:

$$u(\Delta t) = 1/(\sqrt{2\pi}\sigma_p)\exp[-\Delta t^2/(2\sigma_p^2)] \ . \qquad (11)$$

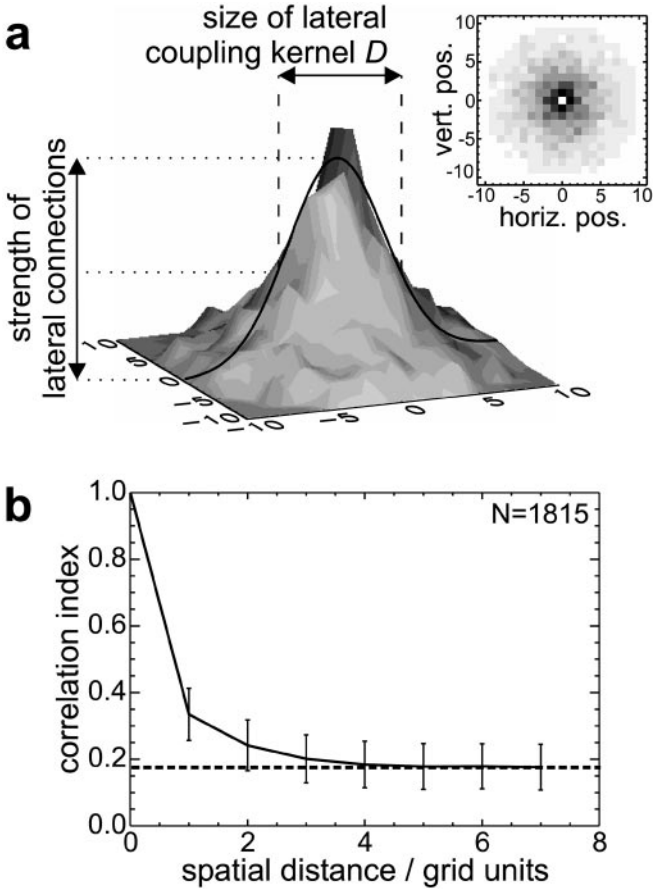

Fig. 4a,b. Scenario A: **a** Average spatial coupling profile between level-1 neurons after learning. Synaptic strength to neighboring neurons is maximal and decays with increasing distance. The inset shows an intensity plot of the same data (grey scale coding; *black:* highest coupling strength). **b** Correlation index of spike output depends on spatial distance. The average correlation strength introduced by the input is indicated by the *dashed line*

In addition, let us consider the projection from a presynaptic neuron n_j to a postsynaptic one n_i. The spikes of n_j need a time interval Δ_{ij} to reach the synapse; therefore, n_i receives a temporally shifted distribution of spikes $u(\Delta t - \Delta_{ij})$ from n_j. Hence, their relative spike timings (pre- and postsynaptic) are a convolution of the distributions:

$$\tilde{p}_{ij}(\Delta t) = u(\Delta t) * u(\Delta t - \Delta_{ij}) \qquad (12)$$

$$= 1/(2\sqrt{\pi}\sigma_p)\exp[-(\Delta t - \Delta_{ij})^2/(4\sigma_p^2)] \ , \qquad (13)$$

which is also a Gaussian with shifted mean and increased standard deviation. This holds only approximately here because it requires statistical independence, whereas in our model pre- and postsynaptic activities are weakly correlated. However, (13) is not used for simulations, but is introduced for a better understanding of the simulation results. Weight increase only occurs for negative Δt (Fig. 3). Thus, the integral

$$p_{ij} = \int_{-\infty}^{0} \tilde{p}_{ij}(\Delta t)\mathrm{d}\Delta t \ , \qquad (14)$$

gives the probability for increasing the synaptic strength between n_j and n_i. The emergence of the lateral coupling kernel can now be understood if we look at two neurons n_n and n_s with a short axonal delay Δ_{ns} in their connection (Fig. 5a). In this case, p_{ns} is large so that the synapse is strengthened quite often. In contrast, a distant neuron n_l has a long delay, so that p_{nl} is low (Fig. 5a). Since weight increasing events are seldom, the resulting strength will be small after learning has converged. Hence, the spatial coupling kernel depends both on the temporal correlation width among spikes at the (inputs and thus at the) outputs of level-1 neurons and the temporal dispersion introduced along the lateral connections.

3.1.2 Variation in the temporal correlation width of the external input σ_p. This variation results in a proportional change of the spatial width D of the lateral coupling profile. Broader input correlations cause broader coupling profiles (Fig. 6a). If we look at a broadened distribution, of relative spike timings (Fig. 5b, dashed curve), more events comply with the timing condition set by the learning rule. Even for distant neurons the synaptic weights grow and therefore the spatial weight distribution becomes broader.

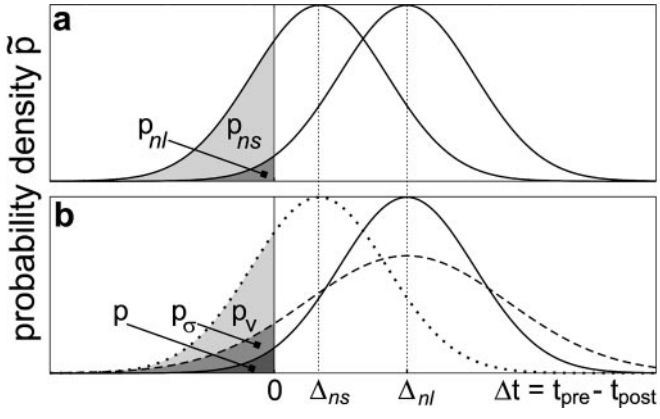

Fig. 5a,b. Probability density functions $\tilde{p}$ of the relative spike timings Δt in the idealized, noiseless case. **a** Connections with a short delay Δ_{ns} have a high probability p_{ns} to be strengthened, while long delay connections have a low probability p_{nl} **b** p is increased by a broader temporal input jitter (p_σ) or a faster axonal velocity (p_v)

3.1.3 Variation of lateral conduction velocity. A narrow coupling width D emerges with a low lateral conduction velocity, and D increases with velocity (Fig. 6b). To explain this effect, let the distance between two neurons n_n and n_l be l_{nl}. As axonal transmission velocity is v_{ax}, the delay between them is $\Delta_{nl} = l_{nl}/v_{ax}$. Increasing the velocity v_{ax} shifts the distribution of relative spike timings p_{nl} in (13) nonlinearly towards zero (Fig. 5b, dotted curve). Thus, the probability of negative time differences, and therefore the number of positive learning events, increases. In the idealized case of infinite conduction velocity, the resulting coupling structure would exhibit no decay at all.

To summarize, the action of increasing lateral propagation velocity and increasing temporal correlation width at the inputs both enlarge the spatial size of the coupling kernel in the lateral network.

3.1.4 Influence of the learning function. The convergence speed of the learning process and the maximal weights depend on the effective duration of the learning window's strengthening epoch (positive part, Fig. 3). If this epoch is elongated beyond the width of the relative spike timings (13), the contribution of random spike correlations to the synaptic weight change increases and, therefore, specific learning is slowed down. If the epoch is shortened, the number of positive learning events decreases (the signal-to-noise ratio for learning effects), so that stable and fast convergence is difficult to obtain. However, in a broad range the duration of the strengthening epoch has no effect on the size of the spatial coupling kernel (Fig. 6c).

3.2 Learning of level-1-to-2 feeding connections (scenarios B, C)

In scenario B (Fig. 1) the distance-dependent connections between level 1 and 2 are learned with the same input as in scenario A, while lateral connectivity among level-1 neurons is absent. After learning, the following structures emerge from the randomly chosen weights (Fig. 7a). The coupling strength of collaterals from the same level-1 neuron decays with distance (Fig. 7b,c). This effect is comparable to the development of the lateral weights at level 1 in scenario A. If neurons at

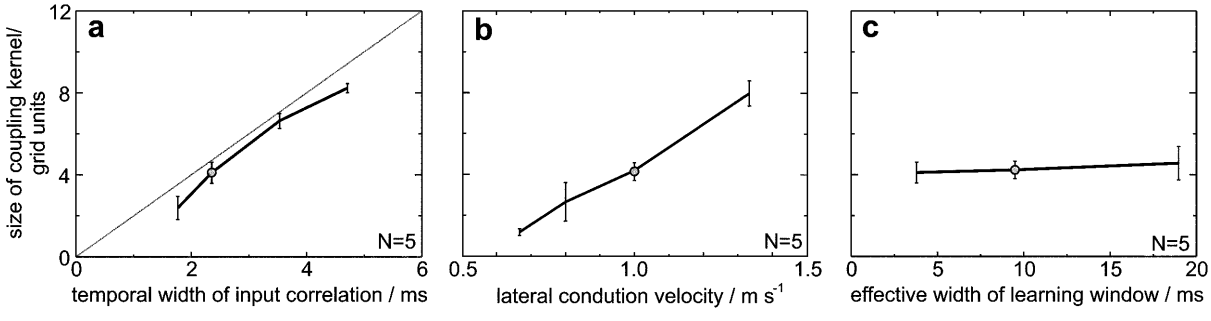

Fig. 6a–c. Scenario A: The width of the synaptic weight profile of the lateral linking connections depends on the temporal width of the input correlations (**a**) and the lateral conduction velocity (**b**), while the decay of the learning window plays only a minor role (**c**). *Grey dots* indicate simulations with identical parameters

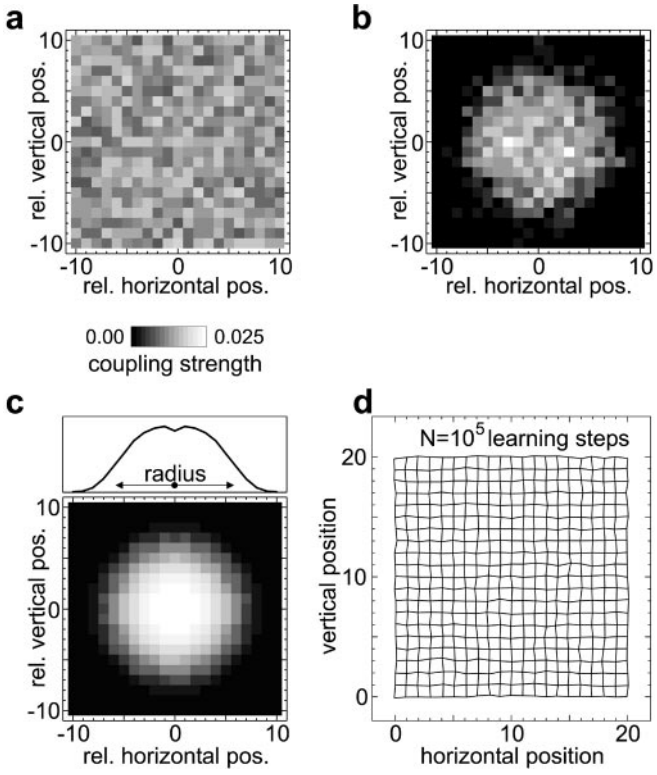

Fig. 7a–d. Scenario B: Synaptic weight distribution at level-2 synapses of feedforward projections from a single level-1 neuron. **a** Example of randomly initialized weights before learning. **b** Example of weight distribution after 10^5 learning steps. **c** Average weight distribution of all level-2 neurons. The dip in the center is due to the decay of the learning window. **d** Spatial distribution of the centers of synaptic weight profiles of level-1-to-2 connections, characterized by the line crossings. In real visual representations these positions would define the centers of cRFs. Note that the retinotopic organization evolves from complete randomness without spatially structured visual input. Only temporal structure was introduced by distance-dependent spike delays

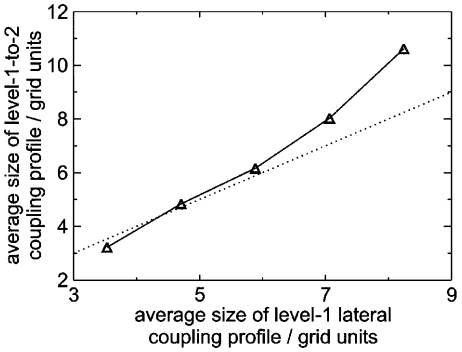

Fig. 8 Scenario C: Size of level-1-to-2 connection profile is correlated with lateral synaptic weight profile of level-1 neurons (simulations with constant level-1-to-2 delays and damped spreading wave activation at level 1, mimicking a learned version of scenario A). Similar relations are obtained with distance-dependent delays between level 1 and 2 in scenario B (not shown)

level 1 generate a correlated spike packet, action potentials, transmitted with short delays, arrive first at retinotopically corresponding level-2 neurons. The evoked EPSPs lead to an increase in the membrane potential and finally, the neuron fires. Since delays are distance-dependent on an evenly spaced grid, few connections with short delays exist. The first EPSPs at a given target neuron are only small in number and are generally not sufficient to evoke a postsynaptic spike. However, additional spikes arriving from more distant neurons eventually cause the neuron to fire. The connections leading to threshold transition are strengthened most, while connections with shorter delays have already fired and therefore have a negative Δt (Fig. 3). Thus, the weights of proximal connections are less strengthened compared to distal ones, which is reflected in the central dip of the weight distribution (Fig. 7c). This dip resembles the decay in the learning function (Fig. 3).

After learning, the centers of the coupling kernels in the neural lattice (corresponding to cRF centers in real systems) are retinotopically well organized (Fig. 7d). This retinotopic sorting is due to the systematic distance-dependent delays in level-1-to-2 connections which define a temporal neighborhood detected by the Hebbian learning function. We would like to note that this retinotopic sorting does not require spatially structured input signals at level 1.

In scenario C (Fig. 1) identical delays in all level-1-to-2 connections are used, and learning started with a broad coupling distribution in the feedforward connections. External inputs are spatially localized blobs of spreading (wave-like) spike activity presented sequentially at random positions (7). After learning, the centers of the feedforward coupling kernels have maintained their initialized topography and have increased their spatial resolution by reducing their size and, thus, reducing the size of level-2 cRFs. The cRF size is monotonically related to the size of the synchronization field and the corresponding AF size at level 1 (Fig. 8).

4 Discussion

We demonstrate how lateral spike propagation velocity can influence the emergence of spatially confined synaptic weight distributions during Hebbian learning without visual experience. Essential for mimicking the developmental phase in visual cortex are also short (<20 ms) common spike rate fluctuations at its external inputs from the thalamus. As these inputs have no spatially structured correlations in our model, the emerging weight distributions are exclusively due to the temporal dispersion of network spike delays and the temporal width of input correlations. If we relate our model structures to visual cortical areas V1 and V2, the weight distributions of the level-1-to-2 feeding connections determine the cRF size in V2, while the weight distributions of level-1 linking connections (V1) define the potential cortical range of synchronization (its projection to visual space is called the association field or AF).

Our learning function is particularly sensitive to precise spike correlations according to the steep gradient

between the negative (unlearning) and the positive (learning) epoch and its asymmetric shape (Fig. 3). Recent experimental results support its biological plausibility (Markram et al. 1997). Fast and stable convergence is obtained when the random temporal dispersion of the external input correlations and the systematic dispersion introduced by lateral spike conduction are matched to the positive epoch of the learning function.

Other models applied learning to continuous mean firing rates (e.g., Kohonen 1984; Phillips and Singer 1997; Stetter et al. 1997; Wiemer et al. 2000) instead of using discrete spike patterns. The former is appropriate if the correlated signals vary slowly. This assumption does not hold for the temporally precise input correlation in our model, which hardly influences the mean firing rate of single neurons (Kempter et al. 1999). However, models based on mean firing rates can, in principle, also transform temporal dispersion into spatially confined coupling structures by learning. Yet, this is restricted to the slow time scale of rate modulations (Wiemer et al. 2000) and does not work on a millisecond time scale as in our model.

Temporal dispersion and variability due to synaptic and dendritic delays are neglected in our model. Introducing biologically plausible values for them will broaden the size of the coupling kernels at level 1 in scenario A (Fig. 4) and level 2 in scenario B (Fig. 7), accordingly. However, such a broadening effect is already present in our model and is reflected in its results: maintained stochastic input (GWN) to level-1 neurons introduces large variability in activation delays because the membrane potential fluctuates and the threshold can be in any state at any moment. This activation variability is large (>10 ms, Fig. 2) compared to what is expected in cortical neurons from synaptic and dendritic delays (<5 ms) under the conditions of rather constant spike rates as in our simulations (Agmon-Snir and Segev 1993).

Lateral conduction delays in the visual cortex (related to scenarios A and B) have been measured only indirectly. If we fit the lateral profile of signal correlations (Fig. 4) to the cortically measured coupling profiles in V1 and V2 (Eckhorn 1994; Frien and Eckhorn 2000) by changing the lateral conduction velocity and keeping the temporal jitter of correlated input spikes small ($\sigma_{in} = 2.5$ ms), the model proposes a velocity of about 0.7 m/s. This value is difficult to compare with real velocities, e.g., in the monkey visual cortex, for several reasons. First, there is a broad distribution of velocities, according to the different fiber diameters of lateral connections. Second, no direct measurements of intra- and interareal conduction delays are available from monkeys. Third, the fitted velocity from the model depends on the temporal correlation width of its input spikes.

As no direct measurements of lateral intraareal conduction velocities (scenario A) have been made in the monkey striate cortex, they have to be estimated by indirect methods, yielding 0.1 to 0.5 m/s for the dominating velocity in V1 in different preparations (review in Nowak and Bullier 1997).

Interareal delays (scenario B) are also relevant for our present work. We concentrate here on V1-V2 delays. They have been measured in monkey revealing delays of a few milliseconds, mostly due to synaptic delay and integration times (Nowak and Bullier 1997). Their shortness is probably related to the myelination between retinotopically corresponding positions of V1 and V2. However, each V1-V2 axon sends collaterals to V2 targets that are generally not myelinated, so that they conduct as slowly as other lateral intraareal connections (on average at 0.3 m/s).

Summarizing, we have to realize that the measured average velocities are too slow by a factor of about two for directly explaining the above mentioned fit to the lateral coupling kernels in V1 and V2. We have to note, however, that the experimental data were collected from visually experienced animals. Therefore, a variety of arguments can explain the differences. (1) The effective fibers determining AF and cRF sizes are indeed as slow as 0.3 m/s. Then we have to assume that the correlation width (jitter) of the input spike trains is broader by a factor of about two, because larger temporal jitter also causes wider coupling profiles (Fig. 6a). (2) There are few fast conducting fibers determining AF and cRF size while the slower conducting axons play no role in determining size. (3) Visual experience, in particular the spatial correlation of visual object features, reshapes the widths of AFs and cRFs on the basis of stimulus-locked synchronization of the input over the range of average object sizes. (4) Other static and dynamic network properties dominate the emergence of spatial structures of visual function, including dynamics at synapses and dendrites and their potential adaptability (e.g., Markram and Tsodyks 1996). These possibilities are not mutually exclusive and the presently available data are not sufficient for giving realistic weights to any of them.

Acknowledgement. We thank A. Gabriel, M. Pauly, A. Thiel, and in particular an anonymous referee for help in improving earlier versions. This work was supported by the Deutsche Forschungsgemeinschaft, Forschergruppe "Dynamics of Cognitive Representations" to R.E.

References

Agmon-Snir H, Segev I (1993) Signal delay and input synchronization in passive dendritic structures. J Neurophysiol 70: 2066–2085

Allman J, Miezin F, McGuinness E (1985) Stimulus specific responses from beyond the classical receptive field: neurophysiological mechanisms for local-global comparisions in visual neurons. Annu Rev Neurosci 8: 407–430

Barlow HB (1972) Single units and sensation: a neuron doctrine for perceptual psychology? Perception 1: 371–394

Chapman B, Gödeke I, Bonhoeffer T (1999) Development of orientation preference in the mammalian visual cortex. J Neurobiol 41:18–24

Crair MC, Gillespie DC, Stryker MP (1998) The role of visual experience in the development of columns in cat visual cortex. Science 279: 566–570

Eckhorn R (1994) Oscillatory and non-oscillatory synchronizations in the visual cortex and their possible roles in associations of visual features. In: van Pelt J, Corner MA, Uylings HBM,

Lopes da Silva FH (eds), The Self-Organizing Brain. Prog Brain Res, vol 102, pp 405–426
Eckhorn R (1999) Neural mechanisms of scene segmentation: recordings from the visual cortex suggest basic circuits for linking field models. IEEE Trans Neural Networks 10: 464–479
Eckhorn R, Reitboeck HJ, Arndt M, Dicke P (1990) Feature linking via synchronization among distributed assemblies: simulations of results from cat visual cortex. Neural Comput 2: 293–307
Eurich CW, Pawelzik K, Ernst U, Cowan JD, Milton JG (1999) Dynamics of self-organized delay adaptation. Phys Rev Letters 82: 1594–1597
Fox K, Daw N (1992) A model for the action of NMDA conductances in the visual cortex. Neural Comput 4: 59–83
Fox K, Sato H, Daw NW (1989) The location and function of NMDA receptors in cat and kitten visual cortex. J Neurosci 9: 2443–2454
Frien A, Eckhorn R (2000) Functional coupling shows stronger stimulus dependency for fast oscillations than for low frequency components in striate cortex of awake monkey. Cereb Cortex 12: 14–26
Gerstner W, Kempter R, van Hemmen JL, Wagner H (1996) A neuronal learning rule for sub-millisecond temporal coding. Nature 383: 76–78
Gray Cm (1999) The temporal correlation hypothesis of visual feature integration. Neuron 24: 31–47
Hubel DH, Wiesel TN (1962) Receptive fields, binocular interaction, and functional architecture in the cat's visual cortex. J Physiol 160: 106–123
Hubel DH, Wiesel TN (1970) The period of susceptibility to the physiological effects of unilateral eye closure in kittens. J Physiol 206: 419–436
Hüning H, Glünder H, Palm G (1998) Synaptic delay learning in pulse-coupled neurons. Neural Comput 10: 555–565
Juergens E, Eckhorn R (1997) Parallel processing by a homogenous group of coupled model neurons can enhance, reduce and generate signal correlations. Biol Cybern 76: 202–208
Kempter R, Gerstner W, van Hemmem JL (1999) Hebbian learning and spiking neurons. Phys Rev E 59: 4498–4514
Kohonen T (1984) Self-organization and associative memory. Springer, Berlin Heidelberg New York
Markram H, Tsodyks M (1996) Redistribution of synaptic efficacy between neocortical pyramidal neurons. Nature 382: 807–810
Markram H, Lübke J, Frotscher M, Sakmann B (1997) Regulation of synaptic efficacy by coincidence of postsynaptic APs and EPSPs. Science 275: 213–215
Meister M, Wong ROL, Baylor DA, Shatz CJ (1991) Synchronous bursts of action potentials in ganglion cells of the developing mammalian retina. Science 17: 939–943
Miller KD (1994) A model for the development of simple cell receptive fields and the ordered arrangement of orientation columns through activity-dependent competition between ON- and OFF-center inputs. J Neurosci 14: 409–441
Miyashita M, Kim D, Tanaka S (1997) Cortical direction selectivity without directional experience. Neuro Report 8: 1187–1191
Nowak LG, Bullier J (1997) The timing of information transfer in the visual system. Cerebral Cortex 12: 205–231
Penn AA, Wong ROL, Shatz CJ (1994) Neuronal coupling in the developing mammalian retina. J Neurosci 14: 3805–3815
Phillips WA, Singer W (1997) In search of common foundations for cortical computation. Behav Brain Sci 20: 657–722
Riesenhuber M, Poggio T (1999) Are cortical models really bound by the "binding problem"? Neuron 24: 87–93
Ritz R, Gerstner W, Fuentes U, van Hemmem JL (1994) A biologically motivated and analytically soluble model of collective oscillations in the cortex. II. Application to binding and pattern segmentation. Biol Cybern 71: 349–358
Saam M, Eckhorn R, Schanze T (1999) Spatial range of synchronization in visual cortex is determined by lateral conduction velocity and determines RF-size at next processing level. Soc Neurosci Abstr 25: 678
Stetter M, Lang EW, Obermayer K (1997) Synapse clustering can drive simultaneous ON- OFF and ocular-dominance segregation in a model of area 17. In: Artificial Neural Networks ICANN '97, Springer, London, pp 189–194
Weliky M, Katz LC (1999) Correlational structure of spontaneous neuronal activity in the developing lateral geniculate nucleus in vivo. Science 285: 599–604
Wiemer J, Spengler F, Joublin F, Stagge P, Wacquant S (2000) Learning cortical topography from spatiotemporal stimuli. Biol Cybern 82: 173–187
Wong ROL, Oakley DM (1996) Changing patterns of spontaneous bursting activity of on and off retinal ganglion cells during development. Neuron 16: 1087–1095